

Two temperature viscous accretion flows around rotating black holes: Description of under-fed systems to ultra-luminous X-ray sources

S. R. Rajesh¹, Banibrata Mukhopadhyay²

Department of Physics, Indian Institute of Science, Bangalore 560012, India

Abstract

We discuss two temperature accretion disk flows around rotating black holes. As we know that to explain observed hard X-rays the choice of Keplerian angular momentum profile is not unique, we consider the sub-Keplerian regime of the disk. Without any strict knowledge of the magnetic field structure, we assume the cooling mechanism is dominated by bremsstrahlung process. We show that in a range of Shakura-Sunyaev viscosity parameter $0.2 \gtrsim \alpha \gtrsim 0.0005$, flow behavior varies widely, particularly by means of the size of disk, efficiency of cooling and corresponding temperatures of ions and electrons. We also show that the disk around a rotating black hole is hotter compared to that around a Schwarzschild black hole, rendering a larger difference between ion and electron temperatures in the former case. With all the theoretical solutions in hand, finally we reproduce the observed luminosities (L) of two extreme cases — the under-fed AGNs and quasars (e.g. Sgr A^*) with $L \gtrsim 10^{33}$ erg/sec to ultra-luminous X-ray sources with $L \sim 10^{41}$ erg/sec, at different combinations of mass accretion rate, ratio of specific heats, Shakura-Sunyaev viscosity parameter and Kerr parameter, and conclude that Sgr A^* may be an intermediate spinning black hole.

Key words:

accretion, accretion disk — black hole physics — hydrodynamics — radiative transfer — gravitation

¹ rajesh@physics.iisc.ernet.in

² bm@physics.iisc.ernet.in

1 Introduction

It was shown by Shapiro, Lightman & Eardley (1976) that to explain observed hard X-rays e.g. from Cyg X-1 the simple Keplerian accretion disk (Shakura & Sunyaev 1973; Novikov & Thorne 1973) is inappropriate. Hence they proposed a two temperature accretion disk with electron and ion temperatures respectively $\sim 10^9\text{K}$ and $\sim 5 \times 10^{11}\text{K}$. Indeed Eggum et al. (1985) showed that the cool disk flow with a constant viscosity parameter α and Keplerian angular momentum profile, which is optically thick and geometrically thin, collapses.

Paczyński & Wiita (1980) proposed a two component accretion disk which is geometrically thick in the optically thick limit. Subsequently, Rees et al. (1982) introduced hot ion torus model in the optically thin limit and Muchotrzeb & Paczyński (1982) initiated the model of transonic accretion in the sub-Keplerian regime. The idea was further pronounced by Chakrabarti (1996) emphasizing the formation of shock in flows and Mukhopadhyay (2003), Mukhopadhyay & Ghosh (2003; hereafter MG03) showing importance of rotation of the central compact object, in full general relativistic as well as pseudo-general relativistic (Mukhopadhyay 2002) frameworks. In the regime of inefficient cooling Narayan & Yi (1995) introduced a two temperature disk model based on self-similar solutions. Abramowicz et al. (1988), on the other hand, proposed a height-integrated disk flow at super-Eddington accretion rate when the diffusion time scale is longer than the viscous time scale rendering a high optical depth of the flow. Other works which helped in developing the modern accretion disk theory may be named as those by, e.g., Begelman (1978), Liang & Thompson (1980), Eggum, Coroniti & Katz (1988).

The two temperature model by Shapiro, Lightman & Eardley (1976) was significantly hotter than single temperature model of Shakura & Sunyaev (1973). The hot gas which is optically thin, however thermally unstable, is considered to be cooled down through the bremsstrahlung and inverse-Compton processes and therefore could explain various states of Cyg X-1 (Melia & Misra 1993). On the other hand, the “ion torus” model by Rees et al. (1982) could explain AGNs at a low mass accretion rate.

However, none of the models attempt to describe the two temperature flow around a rotating black hole and to understand any effect of nonzero specific angular momentum of the black hole. This is particularly important in understanding the inner disk properties. Moreover, there is no attempt, to best of our knowledge, to understand the variation of profiles of ion and electron temperatures in a wide range of α proposed by Shakura-Sunyaev (1973). For example, while Mandal & Chakrabarti (2005) modeled a two temperature flow, they restricted with static black holes without uncovering specific values

of α required for realistic solutions. Their particular emphasis was how the shock helps in fulfilling the radiative processes, and thus they straight away supplied the compression ratio of the flow at the shock location as an input without solving the set of hydrodynamic equations self-consistently. Recently, following the same approach, Das & Chattopadhyay (2008) computed mass loss from viscous accretion disk in presence of cooling.

Very recently, Ghosh & Mukhopadhyay (2009) and Ghosh et al. (2010) described ultra-luminous sources to under-luminous AGNs based on 2.5-dimensional self-similar solutions of accretion disks. However, they could not include the information of angular momentum of the black hole to the solutions due to very nature of the solution procedure (strict choice of self-similarity). Moreover, in their self-similar approach they could not explore two temperature structure of accretion disks, which eventually is an important factor in determining efficiency of cooling and then luminosity.

In the present paper, we plan to model a two temperature relativistic transonic sub-Keplerian accretion flow. We consider the set of hydrodynamic equations describing disk flows along with the components of cooling processes, particularly bremsstrahlung radiation. This is now easier to work out by using the pseudo-Newtonian potential given by Mukhopadhyay (2002), which is being considered to model accretion flows around rotating black holes for sometimes (e.g. Chan, Psaltis & Feryal 2005; Lipunov & Gorbovskoy 2007; Stuchlik & Kovár 2008; Shafee, Narayan & McClintock 2008; Benson & Babul 2009). However, we neither restrict, unlike Narayan & Yi (1995), to the radiatively inefficient advection dominated regime of self-similarity nor, unlike Mandal & Chakrabarti (2005), to a particular aspect of dynamics, e.g. possible formation of shock. We then focus on two extreme regimes of the disk flow — the under-luminous AGNs and quasars (e.g. Sgr A^*) and ultra-luminous X-ray (ULX) sources (e.g. SS433), to implement our model in explaining their luminosities and extracting fundamental properties, e.g. spin.

In the next section, we present the model equations and outline the procedure to solve them. Subsequently, we discuss the two temperature accretion disk solutions around stellar mass and supermassive black holes, respectively for super-Eddington and sub-Eddington accretion rates, in §3. Section 4 compares the disk flow around a rotating black hole with the flow of similar parameters around a static black hole. Finally we discuss the implications of results with a summary in §5.

2 Model equations describing the system

To compute hydrodynamic variables we strictly follow Chakrabarti (1996), Mukhopadhyay (2003) and MG03, but with the gravitational force [as of Mukhopadhyay (2003)] for a black hole given by Mukhopadhyay (2002). Therefore, without discussing the insight, below we straight away recall the basic equations. Note that throughout we express all the variables having their usual meaning in dimensionless units as described in MG03, unless stated otherwise. Hence

$$\dot{M} = -4\pi x \Sigma \vartheta, \quad (1)$$

where the surface density

$$\Sigma = I_n \rho_{eq} h(x), \quad I_n = (2^n n!)^2 / (2n + 1)! \quad (\text{Matsumoto et al. 1984}), \quad (2)$$

when ρ_{eq} is the density at the equatorial plane and the half-thickness is given by

$$h(x) = c_s x^{1/2} F^{-1/2}. \quad (3)$$

$$\vartheta \frac{d\vartheta}{dx} + \frac{1}{\rho} \frac{dP}{dx} - \frac{\lambda^2}{x^3} + F = 0, \quad (4)$$

when we consider the adiabatic equation of state $P = K\rho^\gamma$ with γ being the ratio of specific heats ranging from 4/3 to 5/3, and following Mukhopadhyay (2002)

$$F = \frac{(x^2 - 2a\sqrt{x} + a^2)^2}{x^3 [\sqrt{x}(x-2) + a]^2}, \quad (5)$$

where a is the specific angular momentum (Kerr parameter) of the black hole. We also define

$$\beta = \frac{\text{gas pressure } P_{gas}}{\text{total pressure } P} = \frac{6\gamma - 8}{3(\gamma - 1)} \quad (\text{e.g. Ghosh \& Mukhopadhyay 2009}), \quad (6)$$

where $P_{gas} = P_i$ (ion pressure) + P_e (electron pressure), such that

$$P = \frac{\rho}{\beta c^2} \left(\frac{kT_i}{\mu_i m_i} + \frac{kT_e}{\mu_e m_i} \right) = \rho c_s^2. \quad (7)$$

Here T_i , T_e are respectively the ion and electron temperatures in Kelvin, m_i the mass of proton in gm, μ_i and μ_e respectively the corresponding effective molecular weight, c the speed of light, k the Boltzmann constant.

$$\vartheta \frac{d\lambda}{dx} = \frac{1}{\Sigma x} \frac{d}{dx} (x^2 |W_{x\phi}|), \quad (8)$$

where

$$W_{x\phi} = -\alpha (I_{n+1} P_{eq} + I_n \vartheta^2 \rho_{eq}) h(x) \quad (\text{Chakrabarti 1996, MG03}), \quad (9)$$

when P_{eq} is the pressure at equatorial plane. Note that we will assume $P_{eq} \sim P$ and $\rho_{eq} \sim \rho$ in obtaining solutions. Here we assume a random isotropic magnetic field in the disk governing α .

$$\frac{\vartheta h(x)}{\Gamma_3 - 1} \left(\frac{dP}{dx} - \Gamma_1 \frac{P}{\rho} \frac{d\rho}{dx} \right) = f Q^+, \quad (10)$$

where

$$\begin{aligned} \Gamma_3 &= 1 + \frac{\Gamma_1 - \beta}{4 - 3\beta}, \\ \Gamma_1 &= \beta + \frac{(4 - 3\beta)^2 (\gamma - 1)}{\beta + 12(\gamma - 1)(1 - \beta)} \\ Q^+ &= \alpha (I_{n+1} P + I_n \vartheta^2 \rho) h(x) \frac{d\lambda}{dx} \quad (\text{Chakrabarti 1996, MG03}), \end{aligned} \quad (11)$$

when Q^+ is the heat generated by viscous dissipation and f the parameter determining the fraction of energy advected into the black hole.

Now combining above equations appropriately we obtain (MG03)

$$\frac{d\vartheta}{dx} = \frac{f_1(x, \vartheta, c_s, \lambda)}{f_2(\vartheta, c_s)}, \quad (12)$$

where $f_1(x, \vartheta, c_s, \lambda)$, $f_2(\vartheta, c_s)$ and the solution procedure in detail are given in MG03 (see also Chakrabarti 1996).

After obtaining the hydrodynamic solutions we plug them into the electron heating equation given by

$$\frac{\vartheta h(x)}{\Gamma_3 - 1} \left(\frac{dP_e}{dx} - \Gamma_1 \frac{P_e}{\rho} \frac{d\rho}{dx} \right) = Q_{ie} - Q^-, \quad (13)$$

where Q_{ie} is the Coulomb coupling (Bisnovatyi-Kogan & Lovelace 2000) given in dimensionful unit as

$$q_{ie} = \frac{8(2\pi)^{1/2} e^4 n_i n_e}{m_i m_e} \left(\frac{T_e}{m_e} + \frac{T_i}{m_i} \right)^{-3/2} \ln(\Lambda) (T_i - T_e) \text{ erg/cm}^3/\text{sec}, \quad (14)$$

n_i and n_e denote the number densities of ion and electron respectively, e the charge of an electron, $\ln(\Lambda)$ the Coulomb logarithm. Then Q^- may be the heat radiated away by the bremsstrahlung, synchrotron processes and inverse Comptonization of soft photons. For the present purpose without a proper knowledge of the magnetic field structure in disk, we assume any radiative loss is due to the bremsstrahlung effect given in dimensionful form as (see Narayan & Yi 1995; Mandal & Chakrabarti 2005 for detailed description, what we do not repeat here)

$$q_{br} = 1.4 \times 10^{-27} n_e n_i T_e^{1/2} (1 + 4.4 \times 10^{-10} T_e) \text{ erg/cm}^3/\text{sec}. \quad (15)$$

However, in future we plan to include other components of cooling processes, e.g. synchrotron, inverse-Compton effect to make the model more general (Sinha, Rajesh & Mukhopadhyay 2009; Rajesh & Mukhopadhyay 2009). Important point to note is that in principle one should solve all the five conservation equations simultaneously to obtain the solution (e.g. Sinha, Rajesh & Mukhopadhyay 2009). However, for the present purpose we simply feed the solutions of the hydrodynamic set into the electron energy conservation equation and obtain the electron temperature. We take the present analysis as an exploratory study. If we find that in a wide range of α , as well as in the range of Kerr parameter, the solutions vary noticeably bringing important insights, then we would like to analyze the detailed general solutions by solving the five coupled equations (1), (4), (8), (10), (13) (Rajesh & Mukhopadhyay 2009) simultaneously.

As the flow is considered to be of two temperatures, at the sonic radius x_c the electron temperature T_{ec} needs to be specified, along with corresponding specific angular momentum λ_c of the disk. Note that one has to self-consistently adjust the set of values x_c, λ_c, T_{ec} to obtain solutions connecting outer boundary and black hole event horizon through x_c . Moreover, γ of the flow to be specified according to \dot{M} — higher the \dot{M} , higher the rate of supply of radiation, lower the γ is and vice versa. The outer boundary corresponds to the radius x_o where $\lambda/\lambda_K = 1$. (λ_K being the specific angular momentum of the flow when the centrifugal force is same as gravitational force). Throughout in the text, we quote x_o as the Keplerian to sub-Keplerian transition radius, while we essentially restrict to the inner sub-Keplerian disk.

Below we discuss the solutions particularly for: (1) super-Eddington accretion around stellar mass black holes, (2) sub-Eddington accretion around super-massive black holes.

3 Super- and sub-Eddington accretion around black holes

3.1 Super-Eddington accretion around stellar mass black holes

The “radiation trapped” accretion disk can be attributed to the radiatively driven outflows or jets. This presumably occurs when the accretion rate is super-Eddington (Lovelace et al. 1994, Begelman et al. 2006, Fabbiano 2004, Ghosh & Mukhopadhyay 2009), as seen in ULX sources such as SS433 (with luminosity $\gtrsim 10^{40}$ erg/sec or so; Fabrika 2004). In order to describe such sources, the models described below are the meaningful candidates.

We choose the accretion rate $\dot{M} = 10$ (throughout, the accretion rate is expressed in Eddington units) and mass of the black hole $M = 10$ (throughout, the mass of black hole is expressed in units of solar mass) and obtain solutions for three values of $\alpha = 0.2, 0.01, 0.0005$ around nonrotating (Schwarzschild) and rotating (Kerr with $a = 0.998$) black holes.

3.1.1 Schwarzschild black holes

We first consider flows around static black holes where the Kerr parameter $a = 0$. Figure 1 shows the behavior of flow variables as functions of radial coordinate for $\alpha = 0.2, 0.01, 0.0005$. Higher the α , lower the residence time of the flow is, which results in a hotter flow with a larger f . Therefore we choose the corresponding f appropriately. Note that Narayan & Yi (1995) chose strongly advection dominated hot flows with $f = 1$. However, for the present purpose, we neither consider such an extreme case nor prefer to restrict with advection dominated flows. We rather like to consider flows of general advective paradigm. The sets of input parameters for the model cases described here are given in Table 1. Figure 1a verifies that a lower α corresponds to a lower rate of energy momentum transfer which implies a higher residence time of the flow in the sub-Keplerian regime. As a result, the radial velocity shows a stronger centrifugal barrier for a lower α . As a consequence, Fig. 1b shows that x_o recedes further out for a lower α . Figure 1c shows the bremsstrahlung cooling profile. Naturally the total emission is higher for the flow with a lower α due to a higher residence time before plunging into the black hole. Therefore, the computed luminosity given in Table 1 is higher for a flow of lower α , compared to that of a higher α with a similar parameter set. Note that

while a high α flow might generate higher dissipative energy compared to a low α flow, due to a lower residence time the former flow (with $\alpha \sim 0.2$) could not radiate out completely before plunging into the black hole and thus hotter. In this case, even the Keplerian-sub-Keplerian transition region is of two temperatures, unlike flows with lower α . Interestingly, in the vicinity of black hole the electron temperature goes down, while the ion temperature goes up. This is because very strong advection close to the black hole renders a weaker ion-electron coupling. This in turn hinders the transfer of energy from ions to electrons attributing ions to remain hot, while electrons continue to cool down further by radiative processes. Hence, the difference between ion and electron temperatures is higher for a higher α obviously. However, as was shown by Yuan (2001) and Mandal & Chakrabarti (2005), while close to the black hole the advective heating to electrons becomes stronger, density of the flow increases sharply. This results in the increase of the cooling effects as well, which dominates the advective heating. As electrons are decoupled from ions at this regime, their temperature goes down.

3.1.2 *Kerr black holes*

The specific angular momentum (Kerr parameter) for rotating black holes is chosen to be $a = 0.998$. As discussed earlier (Mukhopadhyay 2003), the angular momentum of the flow around a rotating black hole should be smaller compared to that around a static black hole. This reassembles advancing x_o , which decreases the size of zone of present interest (see Fig. 2b). As the flow angular momentum decreases significantly (see Table 1), the centrifugal barrier completely disappears as shown in Fig. 2a. Thus the infall time is shorter compared to that around a static black hole attributing a smaller residence time of the flow in an element of disk hindering cooling processes to complete. Therefore, the entire disk is hotter compared to that around a static black hole and, hence, even for $\alpha = 0.01$ the transition zone is of two temperatures, as shown in Fig. 2d. Important point to note from Fig. 2c is that the decrease of residence time, close to the black hole event horizon, hinders bremsstrahlung process severely which renders a sharp downfall of bremsstrahlung radiation, compared to that around a static black hole shown in Fig. 1c. As a result, the electron remains hotter compared to that around a nonrotating black hole.

The disk luminosity around a rotating black hole decreases compared to that of a static black hole when α is high. This is because, the relatively less radiative emission is in the former flow when the disk size itself is smaller, as is the case of high α compared to a flow of low α . However, a higher a corresponds to a smaller λ which in turn decreases ϑ at a particular radius of the inner edge of disk, when the inner edge is stretched in, compared to that around a Schwarzschild black hole. Therefore, at a low α , this results in the increase of residence time and then radiative loss of the flow before plunging into the

black hole. Therefore, the luminosity increases compared to that from a disk around a static black hole. See the luminosity column in Table 1.

3.2 *Sub-Eddington accretion around supermassive black holes*

The under-luminous AGNs and quasars (e.g. Sgr A^*) had been attempted to describe by Narayan & Yi (1995) where the flow is expected to be substantially sub-critical/sub-Eddington with a very low luminosity ($\gtrsim 10^{33}$ erg/s). Therefore the cases described below could be potential models in order to describe under-luminous sources.

We choose, primarily, $\dot{M} = 0.01$ and $M = 10^7$ and obtain solutions for three values of $\alpha = 0.2, 0.01, 0.0005$ around nonrotating (Schwarzschild) and rotating (Kerr with $a = 0.998$) black holes.

3.2.1 *Schwarzschild black holes*

Table 2 lists the sets of input parameters. Naturally a disk around a supermassive black hole will have much lower density compared to that around a stellar mass black hole. Hence, the bremsstrahlung radiation is expected to be less efficient leading to a radiatively inefficient flow, particularly for a sub-Eddington accretion flow compared to a super-Eddington flow around a stellar mass black hole. However, the velocity profiles shown in Fig. 3a appear similar to that around a stellar mass black hole, except with a stronger centrifugal barrier. Due to dominance of gas (because of lack of supply of matter and then radiation), γ is higher and the disk appears puffed up and quasi-spherical further away compared to that around a stellar mass black hole. Naturally x_o recedes (Fig. 3b), where the hot flow is of two temperatures unless α is very small rendering a high residence time of matter in the disk which results in a relatively higher luminosity, given by Table 2. However, as the disk around a supermassive black hole and the infall time scale of the matter therein is very large, the total luminosity is only two orders of magnitude lower, at the most, compared to that of stellar mass cases described above, listed in Table 2.

3.2.2 *Kerr black holes*

The specific angular momentum of black hole is chosen to be $a = 0.998$. The basic hydrodynamic properties, particularly the velocity profiles, are similar to that around stellar mass black holes, except, like Schwarzschild cases, x_o recedes, as explained above, shown in Fig. 4. As discussed in §3.1.2, a higher a corresponds to a smaller λ which in turn advances x_o compared to that of the corresponding Schwarzschild case. As the outer edge of sub-Keplerian flow is

relatively closer to the event horizon for a rotating black hole, due to stronger gravitational force ions are hotter and hence the flow is of two temperatures therein, even for $\alpha = 0.0005$. For similar reasons, as explained in §3.1.2, the disk luminosity for a high α decreases compared to that of a static black hole, but increases for a very low α ($= 0.0005$).

3.2.3 Under-luminous AGNs

None of the above cases reveal the luminosity of an under-luminous source, e.g. Sgr A*. Note that the computed luminosity strongly depends on the mass of the black hole and the supplied rate of accretion. If we choose $M = 4.5 \times 10^6$ (Ghez et al. 2008, Reid et al. 2008) and $\dot{M} \lesssim 0.00001$ (Marrone et al. 2007), then the luminosity tallies perfectly with that observed from Sgr A*, particularly for a highly viscous flow (as is predicted by e.g. Narayan et al. 1995) around a rotating black hole in a narrow range of the Kerr parameter a . Table 3 shows how the luminosity varies with the change of α , a , as well as f . Note that we predict the possible value of a based on the extreme advection dominated cases (Narayan & Yi 1995) when f is strictly unity, as well as from general advective paradigm with $0.5 \lesssim f \lesssim 0.7$. Interestingly, for $f < 1$, while $a \sim 0.2$ for a very highly viscous flow with $\alpha \sim 0.2$, it could be in a range $0.2 - 0.5$ when $\alpha \sim 0.05$. However, for advection dominated flows, $a \sim 0.2$. This argues Sgr A* for a rotating black hole with an intermediate spin $0.2 \lesssim a \lesssim 0.5$.

4 Comparison between flows around Schwarzschild and Kerr black holes

From above discussions, we have already got an idea of basic differences between flows of same physical parameters (e.g. α , \dot{M} , γ) around static and rotating black holes of same mass. Here we present a one to one comparison for super-Eddington flows around stellar mass black holes. While, due to general relativistic effects, a disk around a rotating black hole is stretched further in, the transition zone advances quite a bit. Therefore, the total size of sub-Keplerian disk decreases.

From Fig. 5a it is clear that the velocity gradient of inner disk flow around a rotating black hole is less steeper compared to that around a nonrotating black hole, e.g. in the vicinity of $x = 2$, which is the event horizon for the latter case. Therefore, the radial velocity is lower in the former flow at inner disk radii. However, the situation is opposite far away when the sub-Keplerian flow ends at a smaller radius for a rotating black hole and hence the disk is hotter and of two temperatures therein (Fig. 5d), unlike the Schwarzschild case. Indeed

the centrifugal barrier disappears for $a = 0.998$. The radiative loss (Fig. 5c) also shows opposite trends between flows around Kerr and Schwarzschild black holes, particularly at the inner edge, as explained in §3.1.2.

5 Discussion and Summary

We have modeled two temperature accretion flows around black holes. We particularly focus on how the flow properties vary in a wide range of α , and between nonrotating and rotating black holes. In this exploratory study, for simplicity, we consider only the bremsstrahlung radiation as a cooling mechanism. As the solutions for a low α ($= 0.0005$) to a very high α ($= 0.2$) reveal a significant variation of properties/luminosities, in near future we plan to analyze more general solutions including all the possible cooling mechanisms (Sinha, Rajesh & Mukhopadhyay 2009; Rajesh & Mukhopadhyay 2009).

In obtaining associated hydrodynamic solutions needed for computing the bremsstrahlung radiation and then the electron temperature profile, we have strictly followed the earlier works (Chakrabarti 1996; MG03). The temperature of the flow depends on the accretion rate. If the accretion rate is low and thus flow is radiatively inefficient (or less efficient), then the disk is hot. Such a hot flow is being attempted to model since the work by Shapiro, Lightman & Eardley (1976) when it was assumed that $Q^+ \sim Q^-$ locally and thus $f \rightarrow 0$. While the model successfully explained the observed hard X-rays from Cyg X-1, it turned out to be thermally unstable. Latter the hot ion torus model was proposed by Rees et al. (1982) choosing $f < 1$. In the similar spirit Narayan & Yi (1995) proposed the two temperature solution in the regime of $f \rightarrow 1$ when advection is very strong and then Yuan (2001) modified it relaxing the constraint on the accretion rate. Mandal & Chakrabarti (2005) proposed another two temperature disk solution where the ion temperature could be as high as $\sim 10^{12}$ K. However, their particular emphasis was to understand the effect of shock to the cooling mechanisms. They do not carry out a complete analysis of the flow. The present paper, to best of our knowledge, describes for the first time the two temperature accretion flows around *rotating* black holes in a wide range of α .

In order to understand the implications of our solutions, we have chosen two extreme natural cases, namely observed ULX and under-luminous sources which are respectively flows around stellar mass and supermassive black holes. Interestingly the present model is able to explain the observed luminosities for both the sources, as listed in Tables 1,2,3. It is revealed that at a very low mass accretion rate, $\dot{M} \lesssim 0.00001$, around a rotating supermassive black hole of $M \gtrsim 10^6$, the luminosity comes out to be $L \gtrsim 10^{33}$ erg/sec, which is indeed similar to the observed luminosity from an under-luminous source Sgr A*. Note

that the computed L increases (higher than that we observe from under-fed sources) not only due to increase of M and \dot{M} , but also for $a \rightarrow 0$. Therefore, we argue Sgr A^* for a spinning black hole, presumably with a intermediate spin $a \lesssim 0.5$. On the other hand, when we have considered a stellar mass black hole at a super-Eddington mass accretion rate, $\dot{M} = 10$, the model reveals $L \sim 10^{41}$ erg/sec which is similar to the observed luminosity from ULX sources. If the mass of the source is considered to be $M = 10$, then the flow must be highly viscous in order to attribute observed luminosity, according to the cases considered here.

Note that around a rotating black hole the flow angular momentum decreases and thus the radial velocity increases. This in turn reduces the residence time of sub-Keplerian flow hindering cooling processes to complete. This flow with a high viscosity is then expected to be low luminous compared to that around a static black hole. However, the luminosity also depends on the value of α . Lowering α of the flow increases residence time of matter in the disk which helps in cooling processes to complete, switching over a low luminous flow to a high luminous one, when particularly the inner edge, which is radiatively most efficient in the disk, stretches in around a rotating black hole. This feature may help in understanding the transient X-ray sources.

In all the cases, the ion and electron temperatures merge or tend to merge at around transition radius, particularly for a high \dot{M} . This is because, electrons are in thermal equilibrium with ions and thus virial around the transition radius. As the flow advances in the sub-Keplerian regime, the ions become hotter and the corresponding temperature increases, rendering the ion-electron Coulomb collisions weaker. Electrons, on the other hand, cool down via bremsstrahlung radiation keeping the electron temperature roughly constant upto very inner disk. This reveals the two temperature flow entirely.

Important point to note is that we have neither considered a very low viscosity nor a very low accretion rate when nonthermal processes of transferring energy from ions to electrons could be important (Phinney 1981, Begelman & Chiueh 1988). Instead, the viscous heating rate of ions is much higher than the collective rate of nonthermal heating of electrons, unless α is too small. Therefore, our assumption of coupling between ions and electrons due to the Coulomb scattering throughout is justified. However, the process of transferring energy to electrons through anisotropic pressure due to magnetorotational instability in collisionless plasma (Sharma et al. 2007) may be effective, particularly for the low mass accretion rate, which we have neglected in the present work.

Now one should try to understand the radiation emitted from the two temperature flows and to model the corresponding spectra. This will be very useful in order to explain observed data.

Acknowledgments

The authors would like to thank the referee for bringing in attention to recent papers discussing mass and accretion rate of Sgr A^* . This work is partly supported by a project, Grant No. SR/S2HEP12/2007, funded by DST, India. One of the authors (SRR) acknowledges the Council for Scientific and Industrial Research (CSIR; Government of India) for providing a research fellowship.

References

- Abramowicz, M. A., Czerny, B., Lasota, J. P., & Szuszkiewicz, E. 1988, ApJ, 332, 646.
- Begelman, M. C. 1978, MNRAS, 184, 53.
- Begelman, M. C., & Chiueh, T. 1988, ApJ, 332, 872.
- Begelman, M. C., King, A. R., & Pringle, J. E. 2006, MNRAS, 370, 399.
- Benson, A. J., & Babul, A. 2009, MNRAS (to appear); arXiv0905.2378.
- Bisnovatyi-Kogan, G. S., & Lovelace, R. V. E. 2000, ApJ, 529, 978.
- Chakrabarti, S. K. 1996, ApJ, 471, 237.
- Chan, C., Psaltis, D., & Ozel, F. 2005, ApJ, 628, 353.
- Das, S., & Chattopadhyay, I. 2008, NewA, 13, 549.
- Eggum, G. E., Coroniti, F. V., & Katz, J. I. 1985, ApJ, 298, 41.
- Eggum, G. E., Coroniti, F. V., & Katz, J. I. 1988, ApJ, 330, 142.
- Fabbiano, G. 2004, RMxAC, 20, 46.
- Fabrika, S. 2004, ASPRv, 12, 1.
- Ghez, A. M., et al. 2008, ApJ, 689, 1044.
- Ghosh, S., & Mukhopadhyay, B. 2009, RAA, 9, 157.
- Ghosh, S., & Mukhopadhyay, B., Krishan, V., & Khan, M. 2010, NewA, 15, 83; arXiv:0906.0149.
- Gilfanov, M., Churazov, E., & Sunyaev, R. 1997, LNP, 487, 45.
- Liang, E. P. T., & Thompson, K. A. 1980, 240, 271.
- Lipunov, V., & Gorbovskoy, E. 2007, ApJ, 665, 97.

- Lovelace, R. V. E., Romanova, M. M., & Newman, W. I. 1994, *ApJ*, 437, 136.
- Mandal, S., & Chakrabarti, S. K. 2005, *A&A*, 434, 839.
- Marrone, D. P., Moran, J. M., Zhao, J.-H., & Rao, R. 2007, *ApJ*, 654, 57.
- Matsumoto, R., Kato, S., Fukue, J., & Okazaki, A. T. 1984, *PASJ*, 36, 71.
- Melia, F., & Misra, R. 1993, *ApJ*, 411, 797.
- Muchotrzeb, B., & Paczynski, B. 1982, *AcA*, 32, 1.
- Mukhopadhyay, B. 2002, *ApJ*, 581, 427.
- Mukhopadhyay, B. 2003, *ApJ*, 586, 1268.
- Mukhopadhyay, B., & Ghosh, S. 2003, *MNRAS*, 342, 274; MG03.
- Narayan, R., & Yi, I. 1995, *ApJ*, 444, 231.
- Narayan, R., Yi, I., & Mahadevan, R. 1995, *Nature*, 374, 623.
- Novikov, I. D., & Thorne, K. S. 1973, in *Black Holes, Les Houches 1972 (France)*, ed. B. & C. DeWitt (New York: Gordon & Breach), 343.
- Paczynsky, B., & Wiita, P. J. 1980, *A&A*, 88, 23.
- Phinney, E. S. 1981, in *Plasma Astrophysics*, ed. T. D. Guyenne & G. Levy (ESA SP-161), 337.
- Rajesh, S. R., & Mukhopadhyay, B. 2009, *MNRAS* (to appear); arXiv:0910.4502.
- Rees, M. J., Begelman, M. C., Blandford, R. D., & Phinney, E. S. 1982, *Nature*, 295, 17.
- Reid, M. J., Broderick, A. E., Loeb, A., Honma, M., & Brunthaler, A. 2008, *ApJ*, 682, 1041.
- Shafee, R., Narayan, R., & McClintock, J. E. 2008, *ApJ*, 676, 549.
- Shakura, N., & Sunyaev, R. 1973, *A&A*, 24, 337.
- Shapiro, S. L., Lightman, A. P., & Eardley, D. M. 1976, *ApJ*, 204, 187.
- Sharma, P., Quataert, E., Hammett, G. W., & Stone, J. M. 2007, *ApJ*, 667, 714.
- Sinha, M., Rajesh, S. R., & Mukhopadhyay, B. 2009, *RAA* (to appear); arXiv:0910.4818.
- Stuchlík, Z., & Kovár, J. 2008, *IJMPD*, 17, 2089.
- Yuan, F. 2001, *MNRAS*, 324, 119.

Table 1: Parameters and luminosity L in erg/sec for accretion around stellar mass black holes, when the subscript ‘c’ indicates the quantity at the sonic radius and T_{ec} is expressed in units 10^9K

M	\dot{M}	a	γ	x_c	λ_c	α	f	T_{ec}	L
10	10	0	1.34	5.5	3.2	0.2	0.7	48	8.3×10^{41}
10	10	0	1.34	5.5	3.2	0.01	0.5	43.25	3×10^{42}
10	10	0	1.34	5.5	3.2	0.0005	0.3	43.1	2.7×10^{43}
10	10	0.998	1.34	5.5	1.5	0.2	0.7	50	10^{41}
10	10	0.998	1.34	5.5	1.5	0.01	0.5	48	2.1×10^{42}
10	10	0.998	1.34	5.5	1.5	0.0005	0.3	48	5.7×10^{43}

Table 2: Parameters and luminosity L in erg/sec for accretion around super-massive black holes, when the subscript ‘c’ indicates the quantity at the sonic radius and T_{ec} is expressed in units of 10^9K

M	\dot{M}	a	γ	x_c	λ_c	α	f	T_{ec}	L
10^7	0.01	0	1.5	5.5	3.1	0.2	0.7	2.92	4.2×10^{40}
10^7	0.01	0	1.5	5.5	3.2	0.01	0.5	2.8	6.5×10^{40}
10^7	0.01	0	1.5	5.5	3.2	0.0005	0.3	2.79	2×10^{42}
10^7	0.01	0.998	1.5	5.5	1.5	0.2	0.7	2.85	2.6×10^{39}
10^7	0.01	0.998	1.5	5.5	1.5	0.01	0.5	2.75	6.3×10^{40}
10^7	0.01	0.998	1.5	5.5	1.5	0.0005	0.3	2.75	5.8×10^{42}

Table 3: Parameters and luminosity L in erg/sec for accretion around Sgr A^* , when the subscript ‘c’ indicates the quantity at the sonic radius and T_{ec} is expressed in units of 10^9K , $M = 4.5 \times 10^6$, $\dot{M} \lesssim 10^{-5}$

a	γ	x_c	λ_c	α	f	T_{ec}	L
0	1.53	5.5	3	0.2	0.7	2.85	2.9×10^{33}
0	1.53	5.5	3.1	0.05	0.5	2.85	5.1×10^{33}
0.998	1.53	5.5	1.5	0.2	0.7	3.85	7.5×10^{32}
0.998	1.53	5.5	1.8	0.05	0.5	3.85	1.6×10^{33}
0.5	1.53	5.5	2.1	0.2	0.7	2.85	8×10^{32}
0.5	1.53	5.5	2.3	0.05	0.5	2.85	1.7×10^{33}
0.2	1.53	5.5	2.7	0.2	0.7	2.85	2×10^{33}
0.2	1.53	5.5	2.8	0.05	0.5	2.85	2.7×10^{33}
0	1.53	5.5	2.7	0.2	1	2.85	1.4×10^{33}
0	1.53	5.5	3	0.05	1	2.85	4.5×10^{33}
0.998	1.53	5.5	1.2	0.2	1	3.85	5.7×10^{32}
0.998	1.53	5.5	1.7	0.05	1	3.85	1.5×10^{33}
0.5	1.53	5.5	1.7	0.2	1	2.85	4.9×10^{32}
0.5	1.53	5.5	2.4	0.05	1	2.85	1.2×10^{33}
0.2	1.53	5.5	2.2	0.2	1	2.85	9.1×10^{32}
0.2	1.53	5.5	2.7	0.05	1	2.85	2.5×10^{33}

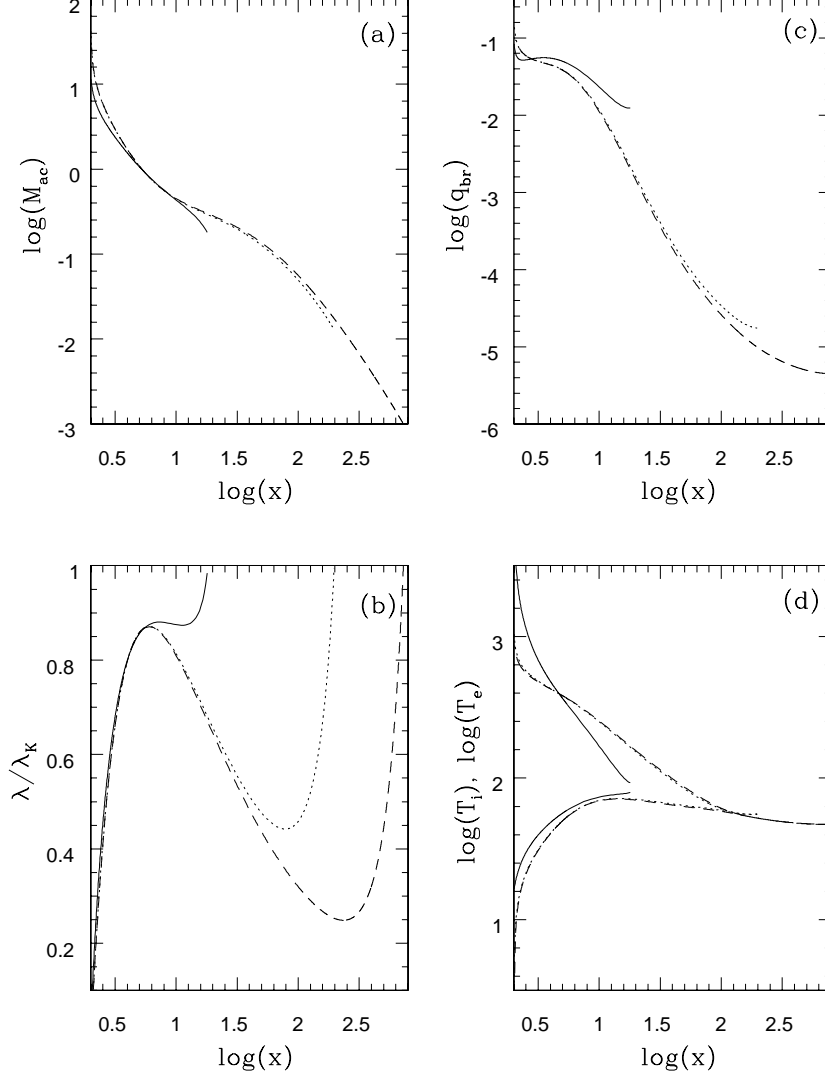


Fig. 1. Variation of (a) Mach number, (b) ratio of disk angular momentum to corresponding Keplerian angular momentum, (c) bremsstrahlung radiation in erg/sec, (d) electron (lower set of curves) and ion (upper set of curves) temperatures in units of 10^9K , as functions of radial coordinate around a Schwarzschild black hole of $M = 10$ and $\dot{M} = 10$. The solid, dotted, dashed curves correspond to $\alpha = 0.2, 0.01, 0.0005$ respectively. The respective parameter sets are given in Table 1 in detail.

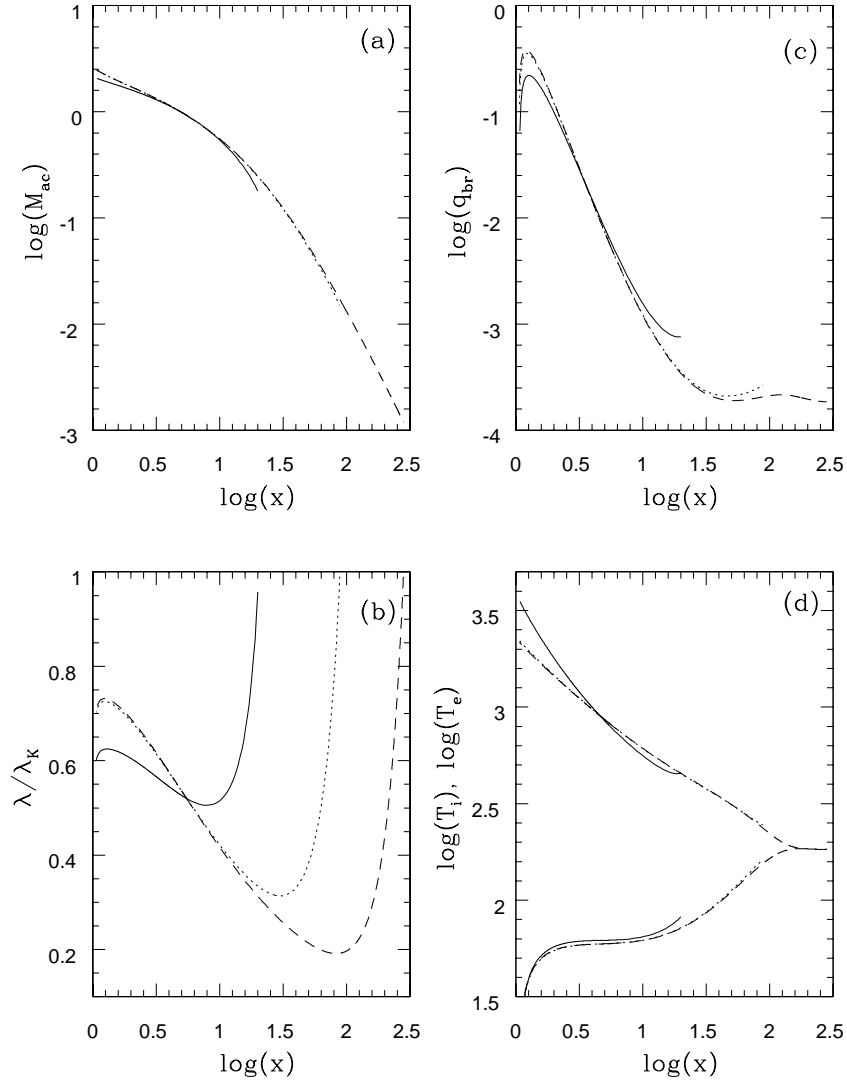


Fig. 2. Same as Fig. 1, except for $a = 0.998$

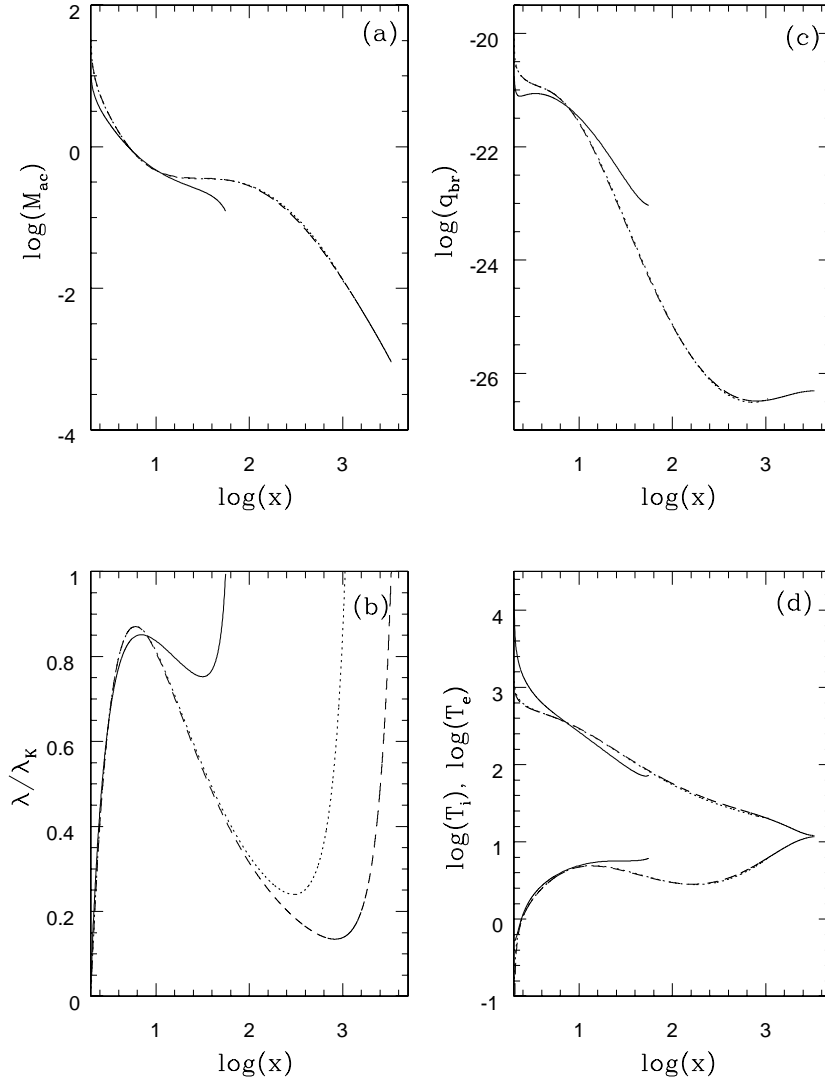


Fig. 3. Same as Fig. 1, except for $M = 10^7$, $\dot{M} = 0.01$. Parameter sets are given in Table 2 in detail.

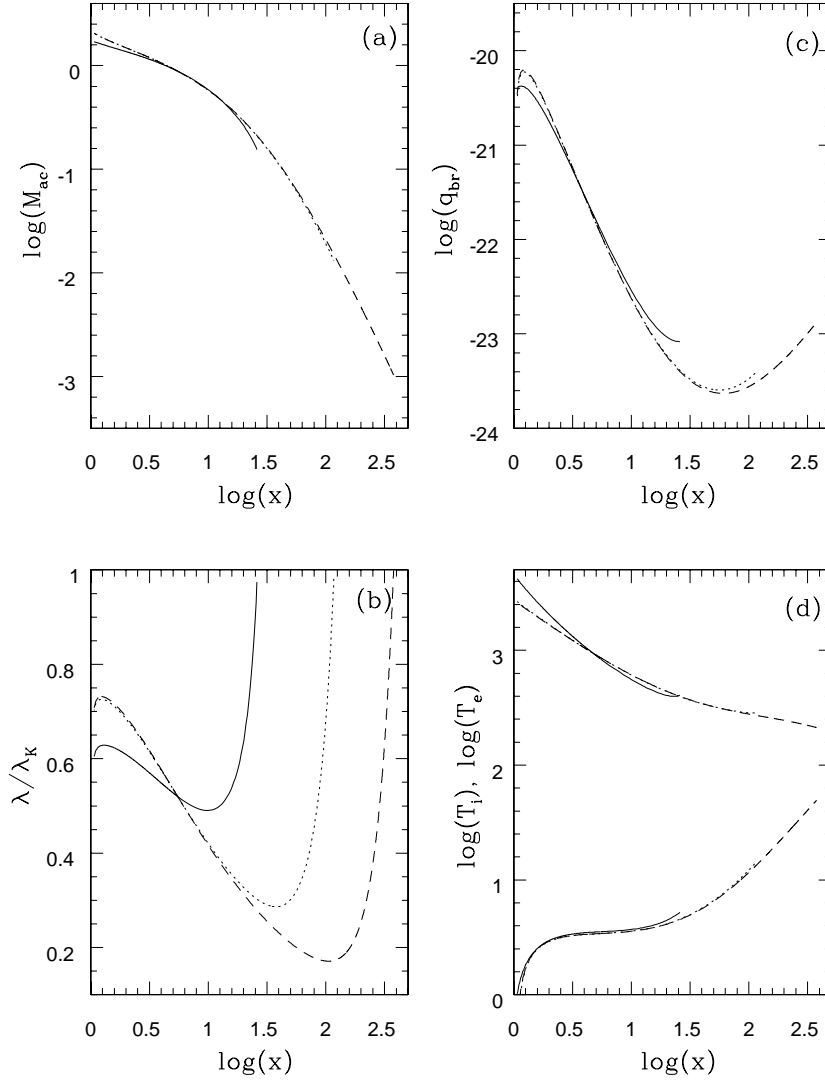


Fig. 4. Same as Fig. 3, except for $a = 0.998$.

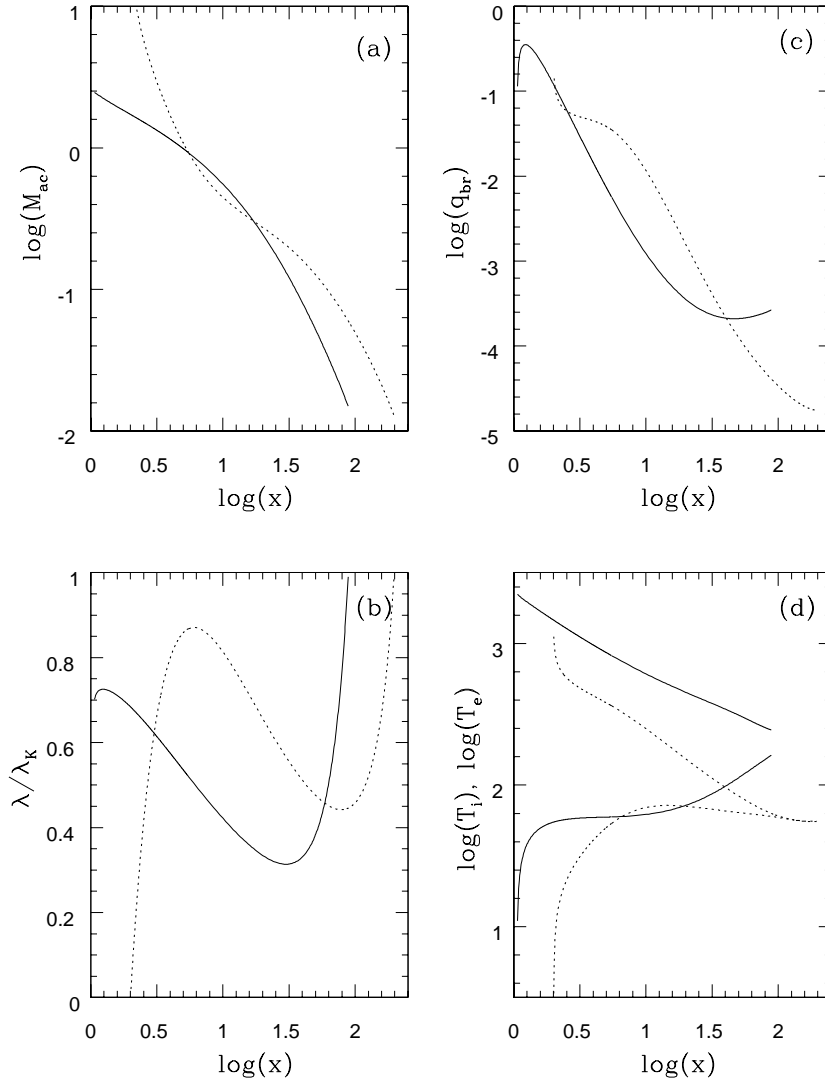


Fig. 5. Variation of (a) Mach number, (b) ratio of disk angular momentum to corresponding Keplerian angular momentum, (c) bremsstrahlung radiation in erg/sec, (d) electron (lower set of curves) and ion (upper set of curves) temperatures in units of 10^9K , as functions of radial coordinate around a black hole of $M = 10$ and $\dot{M} = 10$. The solid, dotted curves correspond to $a = 0.998, 0$ respectively. The respective parameter sets are given in Table 1 in detail.